

## The Effects of Chloride Anions on Corrosion and Passivation Behavior of 254SMO Stainless Steel in Water Absorbed of Blast Furnace Gas (BFG)

Xuan Chen<sup>1</sup>, Qing yun Xiong<sup>2</sup>, Feng Zhu<sup>2</sup>, Hui Li<sup>4</sup>, Dong Liu<sup>4</sup>, Jin ping Xiong<sup>2,3 \*</sup>, Yong Zhou<sup>4 \*</sup>

<sup>1</sup> College of Mechanical and Electrical Engineering, Beijing University of Chemical Technology, Beijing 100029, China

<sup>2</sup> College of Materials Science and Engineering, Beijing University of Chemical Technology, Beijing 100029, China

<sup>3</sup> Beijing Key Laboratory of Electrochemical Process and Technology for Materials, Beijing University of Chemical Technology, Beijing 100029, China

<sup>4</sup> Key Laboratory for Green Chemical Process of Ministry of Education, Wuhan Institute of Technology, Wuhan 430205, China

\*E-mail: [xiongjp@mail.buct.edu.cn](mailto:xiongjp@mail.buct.edu.cn), [zhouyong@wit.edu.cn](mailto:zhouyong@wit.edu.cn)

Received: 24 October 2017 / Accepted: 5 December 2017 / Published: 28 December 2017

The effects of chloride anions ( $\text{Cl}^-$ ) on the corrosion and passivation behavior of 254SMO stainless steel in an electrolyte that was obtained by water absorption of blast furnace gas (BFG) were studied by the electrochemical measurements of potentiodynamic polarization, electrochemical impedance spectroscopy (EIS), potential step and Mott-Schottky plot. The 254SMO steel showed the electrochemical characteristic of spontaneous passivation in the studied electrolyte with different concentrations of  $\text{Cl}^-$ , and the effects of  $\text{Cl}^-$  concentration on the values of passivation current density ( $i_{\text{pass}}$ ), pitting potential ( $E_{\text{pit}}$ ), repassivation potential ( $E_{\text{rep}}$ ), passive film resistance ( $R_f$ ), passive film capacitance ( $CEP_f$ ), donor density ( $N_D$ ) and flat bond potential ( $U_{fb}$ ) presented a certain law but was not very prominent. Further, in the studied  $\text{Cl}^-$  concentration range from 20 g/L to 120 g/L, the 254SMO steel showed good passivation capability in the studied electrolyte, and the passivation capability for the surface of 254SMO stainless steel at the low  $\text{Cl}^-$  concentration was greater than that at the high  $\text{Cl}^-$  concentration.

**Keywords:** 254SMO stainless steel; blast furnace gas (BFG); corrosion; passivation; chloride anion

### 1. INTRODUCTION

Austenitic stainless steels are widely applied in the civil and military industries because of the perfect combination of excellent mechanical performance and good corrosion resistance [1]. Recently,

the modification of conventional austenitic stainless steels and the development of novel austenitic stainless steels are focused on by engineers and technicians continuously [2]. As a novel austenitic stainless steel with the high content of molybdenum (Mo) and nitrogen (N) elements, 254SMO stainless steels have been developed and applied since 1970s, which shows excellent corrosion resistance and passivation capability against the occurrence of pitting corrosion (PC) and crevice corrosion (CC) [3].

At present, studies involving corrosion and protection for 254SMO stainless steels are mainly focused on the following two aspects: the microstructure and composition of passive film on the surface of 254SMO stainless steels and the corrosion behavior of 254SMO stainless steels in various corrosion media [4-10], which is attributed to the advantages of 254SMO stainless steels on comprehensive performance and extensive application. Liu et al. [4] studied the effect of pH on the passivation behavior of 254SMO stainless steel in 3.5 % NaCl solution in the pH range from 0.1 to 5 and reported that the 254SMO steel had good pitting corrosion resistance in 3.5 % NaCl solution, which was very closely associated with the microstructure of passive film according to the XPS analysis. The passive film on the surface of 254SMO stainless steel showed a double layer structure: the out layer was composed of Cr(OH)<sub>3</sub> and Mo (VI), and the inner layer, Cr<sub>2</sub>O<sub>3</sub> and Mo (VI). Meguid et al. [5] studied the critical pitting temperature (*CPT*), critical pitting potential ( $E_{cpit}$ ) and critical protection potential ( $E_{cprot}$ ) of 254SMO stainless steel in chloride solutions with different concentrations of Cl<sup>-</sup> in the temperature range from 30 °C to 100 °C. The authors reported that the values of *CPT*,  $E_{cpit}$  and  $E_{cprot}$  decreased linearly with the logarithm of Cl<sup>-</sup> concentration, and the addition of bromide anions was favorable for the positive shift of  $E_{cpit}$  and  $E_{cprot}$ . Wijesinghe et al. [6] studied the microstructure and composition of passive film formed on the surface of 254SMO stainless steel in borate solution and reported that the passive film was mainly composed of n-type Cr(OH)<sub>3</sub>, possibly with some Ni component, along with n-type Fe<sub>2</sub>O<sub>3</sub>/Fe(OH)<sub>3</sub>. At a positive potential, the Cr (III) was oxidized to a nonsoluble Cr (VI) complex, while at a negative potential, the ferric layer was reduced to p-type FeO. Micheli et al. [7] studied the electrochemical behavior of 254SMO stainless steel in comparison with 316L stainless steel and Hastelloy C276 nickel-based alloy in HCl solutions with different concentrations of Cl<sup>-</sup> and reported that the 254SMO steel presented the comparable corrosion resistance to the C276 alloy when the Cl<sup>-</sup> concentration was less than 1.0 M. The 254SMO steel showed no *CPT* at ambient temperature when the Cl<sup>-</sup> concentration was less than 3.0 M. Further, Micheli et al. [8] also studied the electrochemical behavior of 254SMO stainless steel in H<sub>3</sub>PO<sub>4</sub> solutions in absence and presence of Cl<sup>-</sup> and compared with 316L stainless steel and Hastelloy C276 nickel-based alloy. The authors reported that the 254SMO steel had better corrosion resistance than the 316L steel did and almost the same corrosion resistance as the C276 alloy regardless of the absence and presence of Cl<sup>-</sup>. Odwani et al. [9] studied the corrosion electrochemical behavior of four stainless steels (316L, 317L, 317LNMO and 254SMO) and a titanium alloy (Ti2) in Arabian Gulf seawater by the electrochemical measurements of potentiodynamic polarization and EIS and reported that the corrosion resistance for Ti2 was better than that for stainless steels, and the application of the 254SMO and 317LNMO steels provided better corrosion resistance than the application of the 316L and 317L steels did. However, in the above reports [4-9], the electrolyte component is too simple and the Cl<sup>-</sup> concentration is too low.

In iron and steel industries, blast furnace gas (BFG) needs to be purged into an adsorbed water in order to avoid environmental pollution derived from the direct emission, and the stratum water is usually applied as the adsorbed water because of the wide source and the low cost. However, after the purification process of BFG, the chemical component and the  $\text{Cl}^-$  concentration for the adsorbed water are relatively complicated and high. The high concentration of  $\text{Cl}^-$  may be due to the following two aspects: the inherent presence in stratum water and the entrained component in BFG. However, at present, the published reports on the corrosion and passivation behavior of 254SMO stainless steels in the corrosion media containing the high  $\text{Cl}^-$  concentration are very few, particularly in the electrolyte that was obtained by water absorption of BFG. In this work, a mixed solution containing  $\text{Fe}^{2+}$ ,  $\text{Ca}^{2+}$ ,  $\text{SO}_4^{2-}$ ,  $\text{NO}_3^-$ ,  $\text{PO}_4^{3-}$  and  $\text{Cl}^-$  is applied in order to simulate the actual electrolyte for water adsorption of BFG, and the  $\text{Cl}^-$  concentration is adjusted with the direct addition of NaCl in order to study the effects of chloride anions on the corrosion and passivation behavior of 254SMO stainless steel. The electrochemical measurements of potentiodynamic polarization, electrochemical impedance spectroscopy (EIS), potential step and Mott-Schottky plot are carried out.

## 2. EXPERIMENTAL

### 2.1 Material and solution

The studied material was 254SMO stainless steel with the following chemical composition (wt%): C, 0.013; Cr, 20.27; Ni, 18.03; Mn, 0.45; Si, 0.22; P, 0.020; S, 0.001; Mo, 6.15; N, 0.21; Cu, 0.70, and Fe. Samples were manually abraded up to 1000 grit with SiC abrasive papers, rinsed with de-ionized water and degreased in acetone.

The tested electrolyte for corrosion electrochemical measurements was obtained absorption of BFG by water and was composed of the following components:  $\text{Fe}^{2+}$ , 9.102 g/L;  $\text{Ca}^{2+}$ , 0.332 g/L;  $\text{SO}_4^{2-}$ , 4.260 g/L;  $\text{NO}_3^-$ , 8.161 g/L;  $\text{PO}_4^{3-}$ , 0.078 g/L; and  $\text{Cl}^-$ , 78.500 g/L. In order to study the effect of  $\text{Cl}^-$  concentration, the concentration of  $\text{Cl}^-$  was adjusted with the addition of analytical pure grade NaCl. The studied concentration range of  $\text{Cl}^-$  was from 20 g/L to 120 g/L.

### 2.2 Electrochemical measurement

The electrochemical measurements of potentiodynamic polarization and potential step were carried out using a CS350 electrochemical workstation (China), and the electrochemical measurements of EIS and Mott-Schottky plot were performed using a Princeton 2273 electrochemical instrument (USA). The tested solution was the electrolyte that was obtained by water absorption of BFG with different concentrations of  $\text{Cl}^-$  at pH 4.78. A typical three electrode system was applied for all the electrochemical measurements. The system was composed of a saturated calomel electrode (SCE) as reference electrode, a platinum sheet as counter electrode and the 254SMO sample as working electrode. In the potentiodynamic polarization test, the potential scanning rate and potential scanning range were 0.5 mV/s and from -0.2 V<sub>OCP</sub> and 1.2 V<sub>OCP</sub>, respectively. In the EIS test, a perturbation

potential of 10 mV amplitude was applied in the frequency range from  $10^5$  Hz to  $10^{-2}$  Hz. In the potential step test, a constant potential of 0.5 V<sub>SCE</sub> was applied on the 254SMO sample, and the recording frequency of current density was 5 Hz. In the Mott-Schottky plot test, the potential scanning rate and potential scanning range were 5 mV/s and from -0.6 V<sub>SCE</sub> and 0.6 V<sub>SCE</sub>, respectively.

All of the electrochemical measurements were carried out at 50 °C, and the temperature was controlled with an electro-thermostatic water bath.

### 3. RESULTS AND DISCUSSION

#### 3.1 Potentiodynamic polarization curve

Fig. 1 shows the potentiodynamic polarization curves of the 254SMO samples in the studied electrolyte with different concentrations of Cl<sup>-</sup>. From Fig. 1, in the studied concentration range of Cl<sup>-</sup>, the values of passivation current density for the samples are in the range from  $10^{-6}$  A/cm<sup>2</sup> to  $10^{-5}$  A/cm<sup>2</sup>, indicating that all of the samples presented the electrochemical characteristic of spontaneous passivation in the electrolyte that was obtained by water absorption of BFG [11]. Further, the effects of Cl<sup>-</sup> concentration on the corrosion potential ( $E_{corr}$ ), passivation current density ( $i_{pass}$ ), pitting potential ( $E_{pit}$ ) and repassivation potential ( $E_{rep}$ ) are present, as shown in Fig. 1.

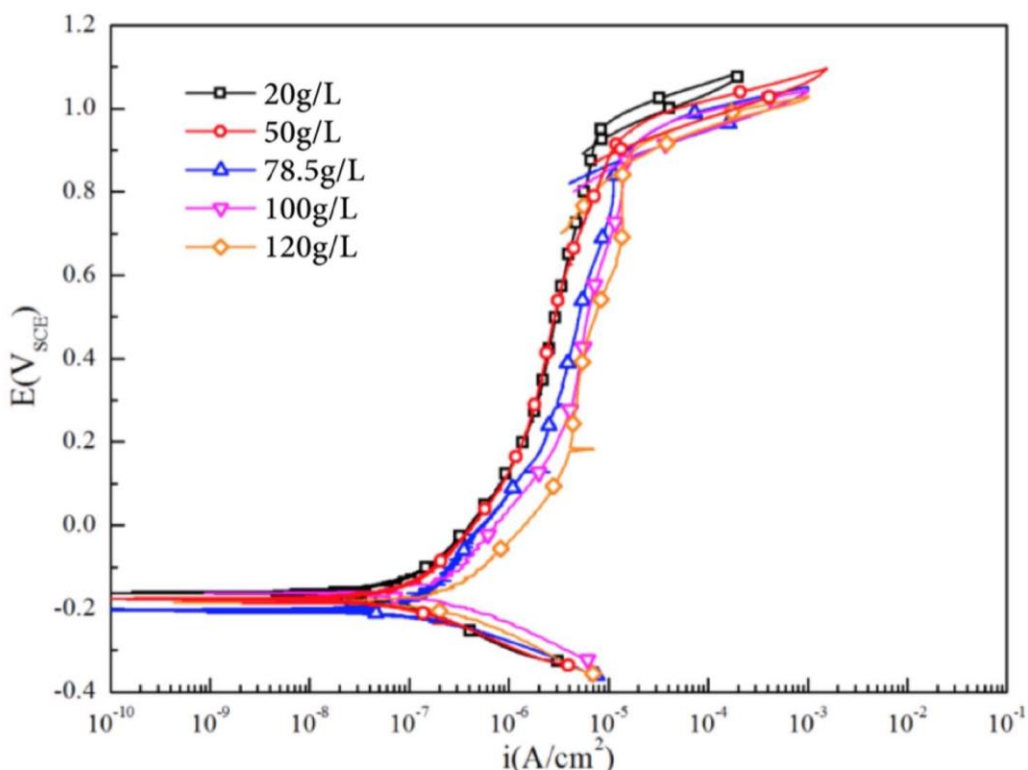


**Figure 1.** Potentiodynamic polarization curves of 254SMO samples in studied electrolyte with different concentrations of Cl<sup>-</sup>.

Table 1 shows the calculated values of  $i_{pass}$ ,  $E_{pit}$ ,  $E_{rep}$  and  $(E_{pit} - E_{rep})$  from the potentiodynamic polarization curves shown in Fig. 1. From Table 1, the values of  $i_{pass}$  increase gradually and the values of  $E_{pit}$  and  $E_{rep}$  move to the negative direction with the increase of  $\text{Cl}^-$  concentration, indicating that the occurrence of spontaneous passivation at the high concentration of  $\text{Cl}^-$  is more difficult than that at the low concentration of  $\text{Cl}^-$ . However, it is noteworthy that in the studied concentration range of  $\text{Cl}^-$ , the values of  $i_{pass}$  are in the same order of magnitude, and the variation for the values of  $E_{pit}$  and  $E_{rep}$  is not very prominent. The results of  $i_{pass}$ ,  $E_{pit}$  and  $E_{rep}$  indicate that the 254SMO steel shows good and stable passivation capability in the corrosion media containing the high concentration of  $\text{Cl}^-$ , which is better than conventional austenitic stainless steels do. Tang et al. [12] tested the potentiodynamic polarization curves of 316L stainless steel in NaCl solutions with the  $\text{Cl}^-$  concentrations from 0.01 M and 0.1 M and reported that the stable passivation capability of the 316L steel was present in the studied concentration range of  $\text{Cl}^-$ . Lv et al. [13] reported that in a simulated occluded cell solution containing chloride anions, the effect of  $\text{Cl}^-$  concentration on the passivation capability of the 304 steel was not very significant when the  $\text{Cl}^-$  concentration was from 1000 mg/L to 3000 mg/L.

At the same time, from the values of  $E_{pit}$  and  $(E_{pit} - E_{rep})$ , the susceptibility of pitting corrosion for 254SMO stainless steel is induced with increased  $\text{Cl}^-$  concentration in the studied electrolyte, which is in agreement with the previous studies on other stainless steels in corrosion media containing chloride anions [12,14,15].

**Table 1.** Calculated values of passivation current density ( $i_{pass}$ ), pitting potential ( $E_{pit}$ ), repassivation potential ( $E_{rep}$ ) and potential difference between pitting potential and repassivation potential ( $E_{pit} - E_{rep}$ ) from potentiodynamic polarization curves.

| [Cl <sup>-</sup> ] (g/L) | $i_{pass}$ ( $\mu\text{A}/\text{cm}^2$ ) | $E_{pit}$ (V <sub>SCE</sub> ) | $E_{rep}$ (V <sub>SCE</sub> ) | $(E_{pit} - E_{rep})$ (V <sub>SCE</sub> ) |
|--------------------------|--|-------------------------------|-------------------------------|---|
| 20                       | 2.44                                     | 1.0622                        | 0.9126                        | 0.1496                                    |
| 50                       | 2.40                                     | 1.0202                        | 0.8906                        | 0.1296                                    |
| 78.5                     | 3.98                                     | 0.9989                        | 0.8716                        | 0.1273                                    |
| 100                      | 5.21                                     | 0.9948                        | 0.8701                        | 0.1247                                    |
| 120                      | 5.56                                     | 0.9787                        | 0.8668                        | 0.1119                                    |

### 3.2 EIS

Fig. 2 shows the EIS of the 254SMO samples in the studied electrolyte with different concentrations of  $\text{Cl}^-$ . From the Nyquist plots shown in Fig. 2a, each plot is composed of only one capacitive loop in the tested frequency range, which is independent on the  $\text{Cl}^-$  concentration in the studied electrolyte. According to our previous study [16], capacitive loops reflect the EIS characteristics of the surface coating/film and the double layer on the working electrode. Further, in this work, the only capacitive loop is due to the presence of passive film on the surface of 254SMO stainless steel. At the same time, the above results also indicate that for the 254SMO steel under the status of OCP, the passive film provides good corrosion resistance and the electrochemical corrosion process is absent on the surface of 254SMO stainless steel.

However, from Fig. 2a, the radius of the capacitive semicircle decreases with the increase of  $\text{Cl}^-$  concentration. At the same time, for the impedance modulus at the low frequency limit of 0.01 Hz shown in Fig. 2b, the modulus value also decreases with increased  $\text{Cl}^-$  concentration. It indicates that in the studied concentration range of  $\text{Cl}^-$ , the passivation capability of 254SMO stainless steel is greater at the low  $\text{Cl}^-$  concentration than at the high  $\text{Cl}^-$  concentration. Further, regardless of  $\text{Cl}^-$  concentration in the studied electrolyte, no other capacitive loop is present in each Nyquist plot, indicating the stable passivation on the surface of 254SMO stainless steel. The above results of EIS are consistent with the results of potentiodynamic polarization: the 254SMO steel shows excellent passivation capability in corrosion media containing the high  $\text{Cl}^-$  concentration.

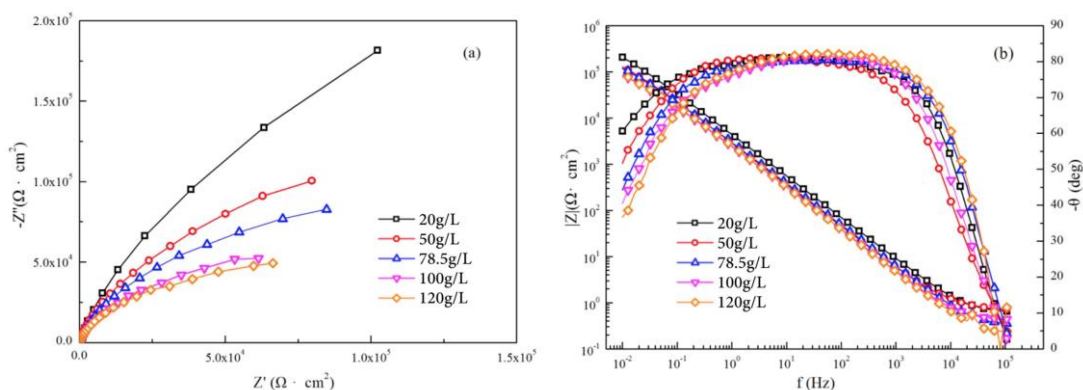


**Figure 2.** EIS of 254SMO samples in studied electrolyte with different concentrations of  $\text{Cl}^-$ : (a) Nyquist plots and (b) Bode plots.

In order to further understand the effect of  $\text{Cl}^-$  concentration on the electrochemical impedance characteristic of the 254SMO steel in the studied electrolyte with different concentrations of  $\text{Cl}^-$ , the equivalent electrical circuit (EEC) fitting was applied. According to the EIS results shown in Fig. 2 and the previous study on electrochemical impedance characteristic [17], the EEC diagram shown in Fig. 3 is selected to fit the EIS results. In Fig. 3,  $R_s$  represents the solution resistance, and  $R_f$  and  $CPE_f$  represent the resistance and the capacitance of passive film, respectively.

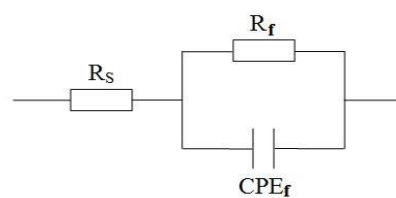


**Figure 3.** Equivalent electrical circuit diagram.

Table 2 shows the fitted values of  $R_f$  and  $CPE_f$  from the EIS shown in Fig. 2. It was reported that the  $R_f$  value reflected the corrosion resistance of passive film for the metal or alloy substrate [18]. From Table 2, the values of  $R_f$  decreases gradually with the increase of  $\text{Cl}^-$  concentration in the studied

electrolyte. On the other hand, it was also reported that the  $CPE_f$  value indicated the actual destructive area on the surface of passive film [18]. Table 2 illustrate that the  $CPE_f$  value for the 254SMO sample at the low  $\text{Cl}^-$  concentration is lower than that at the high  $\text{Cl}^-$  concentration. The above results of  $R_f$  and  $CPE_f$  indicate that the passive film formed at the lower  $\text{Cl}^-$  concentration provides better corrosion resistance than that formed at the high  $\text{Cl}^-$  concentration does.

**Table 2.** Fitted values of resistance and capacitance for passive film from EIS.

| [Cl] (g/L) | $R_f (\Omega \cdot \text{cm}^2)$ | $CPE_f (\text{F}/\text{cm}^2)$ |
|------------|----------------------------------|--------------------------------|
| 20         | $6.731 \times 10^5$              | $2.709 \times 10^{-5}$         |
| 50         | $2.442 \times 10^5$              | $3.152 \times 10^{-5}$         |
| 78.5       | $1.990 \times 10^5$              | $2.981 \times 10^{-5}$         |
| 100        | $1.149 \times 10^5$              | $2.346 \times 10^{-5}$         |
| 120        | $1.109 \times 10^5$              | $5.511 \times 10^{-5}$         |

### 3.3 Potential step

Fig. 4 shows the current transients of the 254SMO samples in the studied electrolyte with different concentrations of  $\text{Cl}^-$ . From Fig. 4, regardless of the  $\text{Cl}^-$  concentration, the current density of each sample decreases gradually with the extension of tested time. However, the initial and terminated values of the current density for the samples at the low  $\text{Cl}^-$  concentration is lower than those for the samples at the high  $\text{Cl}^-$  concentration, indicating that the passivation occurrence is easier at the low  $\text{Cl}^-$  concentration than at the high  $\text{Cl}^-$  concentration.

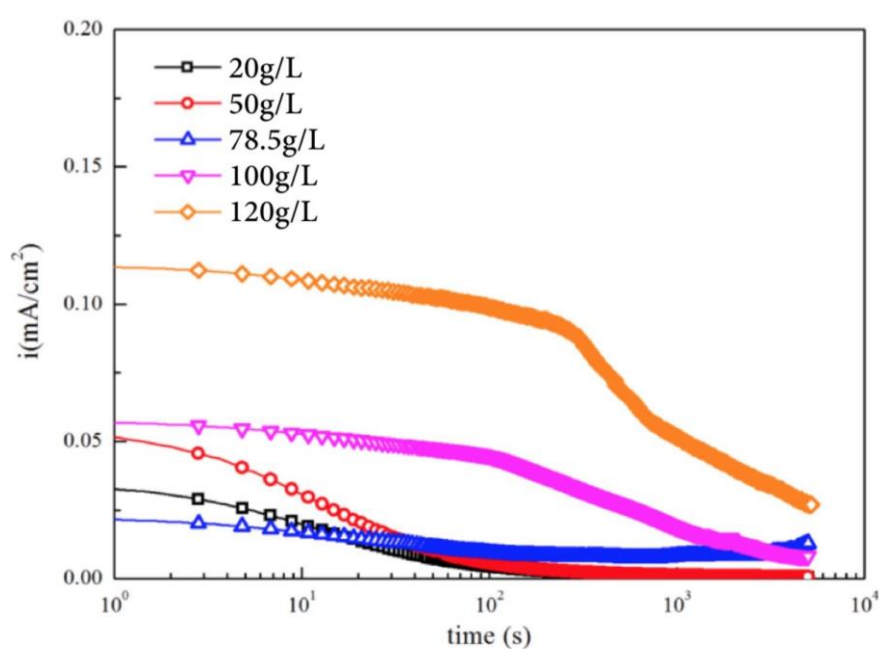


**Figure 4.** Current transients of 254SMO samples in studied electrolyte with different concentrations of  $\text{Cl}^-$ .

### 3.4 Mott-Schottky plot

Fig. 5 shows the Mott-Schottky plots of the 254SMO samples in the studied electrolyte with different concentrations of  $\text{Cl}^-$ . It was reported that the passive film on the surface of metals and alloys could be considered as a semiconductor [19]. From Fig. 5, the slope of the straight line part on each Mott-Schottky plot presents a positive value, suggesting that the passive film on the surface of 254SMO stainless steel is a n-type semiconductor. According to the Mott-Schottky theory for n-type semiconductors [20], the relation between the space charge layer capacitance ( $C_{sp}$ ) and the applied potential ( $E_{apply}$ ) is as follows:

$$\frac{1}{C_{sp}^2} = \frac{2(E_{apply} - U_{fb} - \frac{kT}{e})}{\epsilon \epsilon_0 e N_D} \quad (1)$$

where  $U_{fb}$  represents the flat band potential,  $k$  represents the Boltzmann constant,  $T$  represents the absolute temperature,  $e$  represents the electron charge,  $\epsilon$  is the dielectric constant of the passive film,  $\epsilon_0$  is the permittivity of free space and  $N_D$  is the donor density.

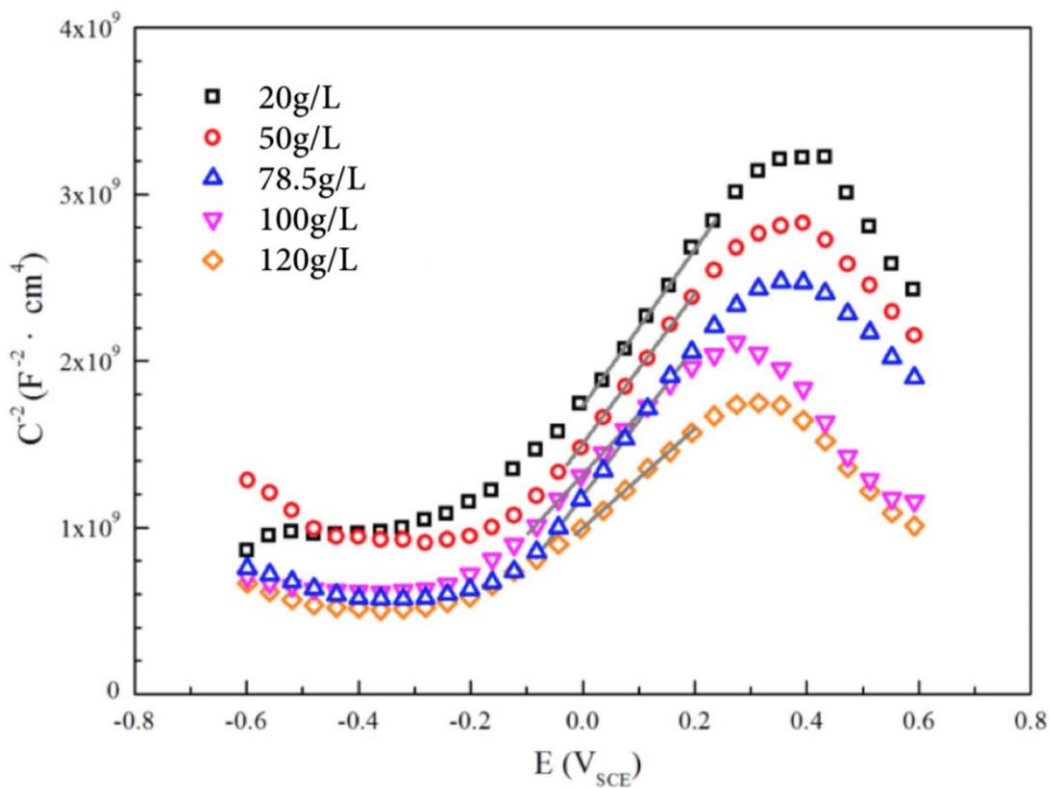


**Figure 5.** Mott-Schottky plots of 254SMO samples in studied electrolyte with different concentrations of  $\text{Cl}^-$ .

In the Equation (1), the values of  $N_D$  and  $U_{fb}$  are the important parameters to reflect the corrosion electrochemical behavior [21]. It was reported that the  $N_D$  value indicated the film defects in the internal of passive film, which could be calculated by the slope of the straight line part on the Mott-

Schottky plot [22]. At the same time, the  $U_{fb}$  value reflected the corrosion susceptibility for metals and alloys in corrosion media, which could be obtained by extrapolation of the Mott-Schottky plot to  $1/C_{sp}^2 = 0$ . Table 3 shows the calculated values of  $N_D$  and  $U_{fb}$  from the Mott-Schottky plots shown in Fig. 5. From Table 3, the values of  $N_D$  increase gradually with the increase of  $\text{Cl}^-$  concentration, indicating the film defects in the passive film formed at the high  $\text{Cl}^-$  concentration is more than that formed at the low  $\text{Cl}^-$  concentration. The more defects in the passive film, the lower corrosion resistance of the material substrate [23]. The results of Mott-Schottky plots are in agreement with the results of potentiodynamic polarization and EIS, indicating that the passivation capability of 254SMO stainless weakens with the increase of  $\text{Cl}^-$  concentration in the studied electrolyte. Similar results on other stainless steels are also reported [24-26].

**Table 3.** Calculated values of donor density ( $N_D$ ) and flat band potential ( $U_{fb}$ ) from Mott-Schottky plots.

| [ $\text{Cl}^-$ ] (g/L) | $N_D$ ( $\text{cm}^{-3}$ ) | $U_{fb}$ (V <sub>SCE</sub> ) |
|-------------------------|----------------------------|------------------------------|
| 20                      | $1.930 \times 10^{21}$     | -0.4012                      |
| 50                      | $2.012 \times 10^{21}$     | -0.3667                      |
| 78.5                    | $2.021 \times 10^{21}$     | -0.3340                      |
| 100                     | $2.501 \times 10^{21}$     | -0.3069                      |
| 120                     | $3.048 \times 10^{21}$     | -0.2676                      |

It is generally accepted that the addition of Mo elements in steel products is favorable for the improvement of corrosion resistance [27]. For example, in the same corrosion media, 316(L) stainless steel usually shows the better corrosion resistance than 304(L) stainless steel does [28]. As a novel austenitic stainless steel with the high content of Mo, the high capability of spontaneous passivation for 254SMO stainless steel is also associated with the presence of Mo element [6]. In this work, from the electrochemical measurement results, the 254SMO steel shows good passivation capability in the electrolyte that was obtained by water absorption of blast furnace gas (BFG) with the  $\text{Cl}^-$  concentration range from 20 g/L to 120 g/L, and the passivation capability decreases with the increase of  $\text{Cl}^-$  concentration.

#### 4. CONCLUSIONS

In this work, the effects of chloride anions on the corrosion and passivation behavior of 254SMO stainless steel in an electrolyte that was obtained by water absorption of blast furnace gas (BFG) were studied by electrochemical measurements. In the studied concentration range of  $\text{Cl}^-$ , the following conclusions were obtained:

(1) The 254SMO steel showed the electrochemical characteristic of spontaneous passivation in the studied electrolyte with different concentrations of  $\text{Cl}^-$ .

(2) The effect of  $\text{Cl}^-$  concentration on the corrosion electrochemical parameters of passivation current density, pitting potential, repassivation potential, passive film resistance and capacitance, donor density and flat bond potential was not very prominent.

(3) The passivation capability for the surface of 254SMO stainless steel at the low Cl<sup>-</sup> concentration was greater than that at the high Cl<sup>-</sup> concentration.

#### ACKNOWLEDGEMENTS

This work is supported by the National Science Foundation of Hubei Province of China (Contract 2016CFB264) and the National Natural Science Foundation of China (Contract 51401150).

#### References

1. A.B. Rhouma, T. Amadou, H. Sidhom and C. Braham, *J. Alloy. Compd.*, 708 (2017) 871.
2. F. Shi, P.C. Tian, N. Jia, Z.H. Ye, Y. Qi, C.M. Liu and X.W. Li, *Corros. Sci.*, 107 (2016) 49.
3. Y. Han, H. Wu, W. Zhang, D.N. Zou, G.W. Liu and G.J. Qiao, *Mater. Design*, 69 (2015) 230.
4. C.T. Liu and J.K. Wu, *Corros. Sci.*, 49 (2007) 2198.
5. E.A. Abd EI Meguid and A.A. Abd EI Latif, *Corros. Sci.*, 49 (2007) 263.
6. T.L.S.L. Wijesinghe and D.J. Blackwood, *J. Electrochem. Soc.*, 154 (2007) C16.
7. L. De Micheli, C.A. Barbosa, A.H.P. Andrade and S.M.L. Agostinho, *Birt. Corros. J.*, 35 (2000) 297.
8. L. De Micheli, A.H.P. Andrade, C.A. Barbosa and S.M.L. Agostinho, *Birt. Corros. J.*, 34 (1999) 67.
9. A.A. Odwani, M. Al-Tabatabaei and A. Abdel-Nabi, *Desalination*, 120 (1998) 73.
10. F.G. Deng, L.S. Wang, Y. Zhou, X.H. Gong, X.P. Zhao, T. Hu and C.G. Wu, *RSC Adv.*, 7 (2017) 48876.
11. Y. Zhou and F.A. Yan, *Int. J. Electrochem. Sci.*, 11 (2016) 3976.
12. Y.M. Tang, Y. Zuo, J.N. Wang, X.H. Zhao, B. Niu and B. Lin, *Corros. Sci.*, 80 (2014) 111.
13. G.C. Lv, C.C. Xu, Y.M. Lv, H.D. Cheng and Z.H. He, *Chin. J. Chem. Eng.*, 16 (2008) 646.
14. X.G. Feng, X.Y. Lu, Y. Zuo, N. Zhuang and D. Chen, *Corros. Sci.*, 103 (2016) 223.
15. Y. Zuo, H.T. Wang, J.M. Zhao and J.P. Xiong, *Corros. Sci.*, 44 (2002) 13.
16. Y. Zhou, J.P. Xiong, F.A. Yan, *Surf. Coat. Tech.*, 328 (2017) 335.
17. Z.Y. Yong, J. Zhu, C. Qiu and Y.L. Liu, *Appl. Surf. Sci.*, 255 (2008) 1672.
18. Q.Y. Xiong, J.P. Xiong, Y. Zhou, F.A. Yan, *Int. J. Electrochem. Sci.*, 12 (2017) 4238.
19. Y.F. Cheng and J.L. Luo, *Appl. Surf. Sci.*, 167 (2000) 113.
20. Y.F. Cheng and J.L. Luo, *Electrochimi. Acta*, 44 (1999) 2947.
21. Y. Zhou, P. Zhang, Y. Zuo, D. Liu and F.A. Yan, *J. Braz. Chem. Soc.*, 28 (2017) 2490.
22. Y. Zhou and Y. Zuo, *J. Electrochem. Soc.*, 162 (2015) C47.
23. Y. Zhou and Y. Zuo, *Appl. Surf. Sci.*, 353 (2015) 924.
24. H. Luo, C.F. Dong, X.G. Li and K. Xiao, *Electrochimi. Acta*, 64 (2012) 211.
25. Q.Y. Xiong, Y. Zhou and J.P. Xiong, *Int. J. Electrochem. Sci.*, 10 (2015) 8454.
26. W.S. Li and J.L. Luo, *Electrochim. Comm.*, 1 (1999) 349.
27. J. Qian, C.F. Chen, H.B. Yu, F. Liu, H. Yang and Z.H. Zhang, *Corros. Sci.*, 111 (2016) 352.
28. A. Pardo, M.C. Merino, A.E. Coy, F. Viejo, R. Arrabal and E. Matykina, *Corros. Sci.*, 50 (2008) 780.